European Journal of Mechanics B/Fluids 30 (2011) 360–370

Contents lists available at ScienceDirect

European Journal of Mechanics B/Fluids

journal homepage: www.elsevier.com/locate/ejmflu

# A turbulence model for Smoothed Particle Hydrodynamics

J.J. Monaghan

*School of Mathematics Sciences, Monash University, Clayton 3800, Australia*

ARTICLE INFO

*Article history:*
Received 24 November 2010
Received in revised form
25 March 2011
Accepted 7 April 2011
Available online 15 April 2011

*Keywords:*
Turbulence
2D box
SPH

ABSTRACT

The aim of this paper is to describe a turbulence model for the particle method Smoothed Particle Hydrodynamics (SPH). The model makes few assumptions, conserves linear and angular momentum, satisfies a discrete version of Kelvin's circulation theorem, and is computationally efficient. Furthermore, the results from the model are in good agreement with the experimental and computational results of Clercx and Heijst for two-dimensional turbulence inside a box with no-slip walls. The model is based on a Lagrangian similar to that used for the Lagrangian averaged Navier–Stokes (LANS) turbulence model, but with a different smoothed velocity. The smoothed velocity preserves the *shape* of the spectrum of the unsmoothed velocity, but reduces the magnitude for short length scales by an amount which depends on a parameter $\epsilon$. We call this the SPH-$\epsilon$ model. The effectiveness of the model is indicated by the fact that the second and fourth order velocity correlation functions calculated using the smoothed velocity and a coarse resolution, are in good agreement with a calculation using a resolution which is finer by a factor 2, and therefore requires 8 times as much work to integrate to the same time.



## 1. Introduction

The subject of this paper is a turbulence model for Smoothed Particle Hydrodynamics (SPH, for a review see [1]). The SPH method was developed for astrophysical applications but has been progressively extended to problems involving incompressible fluids by using either a weakly compressible model of the fluid [2], or by algorithms designed to solve the full incompressible equations [3,4]. In this paper we use the weakly compressible model.

Many of the incompressible flow problems to which SPH has been applied involve the generation of turbulence. An example is the turbulence created in a laboratory dam break problem when the flow strikes the downstream wall of the tank. Standard turbulence models such as the $k-\epsilon$ model have been applied to the SPH simulation of dam break problems [5] with modest success. It seems preferable, however, to construct a turbulence model within the framework of SPH in such a way that general principles such as conservation of energy, momentum and circulation are satisfied.

In this paper we make use of the ideas associated with the Lagrangian averaged Navier–Stokes equations (LANS) explored by Holm and his colleagues [6–12], and for extensive references see [13–15]. In the latter papers, LANS models are studied for two-dimensional fluid turbulence in a periodic domain.

The basic idea of LANS is to determine a smoothed velocity $\widehat{\mathbf{v}}$ by a linear operation on the unsmoothed velocity $\mathbf{v}$, and then determine the Eulerian equations of motion from a Lagrangian where the kinetic energy per unit mass is $\frac{1}{2}\widehat{\mathbf{v}}\cdot\mathbf{v}$. The same idea is used here for an SPH model. The continuum Lagrangian is replaced by a particle Lagrangian, the kinetic energy for a particle $a$ is $\frac{1}{2}m_a\widehat{\mathbf{v}}_a\cdot\mathbf{v}_a$ where $m_a$ is its mass, and the smoothing takes a different form to that involved in the LANS models referenced above. Because the smoothing involves a parameter $\epsilon$ we shall refer to the turbulence model as the SPH-$\epsilon$ model.

The average motion of the fluid is determined by $\widehat{\mathbf{v}}$, and the SPH particles move with this velocity i.e. $\mathrm{d}\mathbf{r}/\mathrm{d}t = \widehat{\mathbf{v}}$. The canonical coordinates for particle $a$ are therefore $\mathbf{r}_a$ and $\widehat{\mathbf{v}}_a$. Lagrange's equations contain extra velocity dependent terms which represent the stresses induced by the smoothing. Once the form of the smoothing is chosen these stresses are determined. The overall effect is to produce a redistribution of energy without dissipation. The equations of motion conserve energy, linear and angular momentum (in the absence of rigid boundaries and external forces), and they satisfy a discrete version of the circulation theorem.

To complete the model we add a viscous dissipation term. We use one of the standard SPH viscosity terms which has been tested for Couette flow [16], and for spin down in a rotating cylinder [1,17]. We simulate the boundary conditions associated with fixed or moving bodies by placing boundary particles on the boundary in a way which is similar to the Immersed Boundary Method of [18,19]. This technique has been shown to give good results for a wide range of problems [17]. The effects of the turbulence on processes such as thermal transport can be estimated using the differences between the smoothed and unsmoothed velocities to determine diffusion coefficients. However, we do not study those processes in this paper.

*E-mail address:* joe.monaghan@monash.edu.

0997-7546/$ – see front matter © 2011 Published by Elsevier Masson SAS.
doi:10.1016/j.euromechflu.2011.04.002

We apply the SPH-$\epsilon$ equations to turbulence in a two-dimensional box with no-slip boundary conditions. This system has been studied both experimentally and numerically [20–24] and is particularly interesting because it shows that the fluid motion with no-slip or stress-free boundary conditions (relevant to many turbulence problems in nature), differs significantly from that with periodic boundary conditions. This includes the formation of vortices, the spectrum, and changes in the angular momentum [20,21,25,26]. The two-dimensional problem also has the advantage that the computational demands are very much less than for a three-dimensional simulation.

The plan of the paper is to discuss the smoothing, and show how it can be formulated so that the linear and angular momentum are conserved in the absence of boundaries and external body forces. We then derive the Euler equations of motion from a Lagrangian and complete the SPH-$\epsilon$ equations by adding the boundary force and viscous terms. We discuss the conditions for the kinetic energy to be positive definite and describe the time stepping scheme. We apply the SPH-$\epsilon$ equations to predict the properties of decaying turbulence initialised by a set of Gaussian vortices. The results, both with and without smoothing, are then compared with those of Clercx et al. [21,22] and Maassen et al. [24] and the effects of smoothing on velocity correlations functions are then discussed.

## 2. Dynamics and smoothing

The Euler equations for the fluid are the Lagrange equations which can be obtained from Eckart's Lagrangian [27] which, for a compressible fluid, takes the form

$$L = \int \rho \left( \frac{1}{2} \mathbf{v} \cdot \mathbf{v} - u(\rho, s) \right) \mathbf{dr}, \tag{2.1}$$

where $u(\rho, s)$ is the internal energy per unit mass associated with the equation of state and $\mathbf{dr}$ denotes a volume element. The internal energy depends, in general, on the density $\rho$ and the entropy per unit mass $s$. For the non-dissipative Lagrangian formulation, the value of $s$ carried by an element of fluid does not vary with time. In this paper we assume each particle has the same entropy. The SPH form of (2.1) is obtained by replacing the integration by a summation over finite mass elements noting that the infinitesimal mass element is $\rho \mathbf{dr}$. We then get

$$L = \sum_b m_b \left( \frac{1}{2} \mathbf{v}_b \cdot \mathbf{v}_b - u(\rho_b, s_b) \right). \tag{2.2}$$

The LANS model replaces (2.1) by

$$L = \int \rho \left( \frac{1}{2} \mathbf{v} \cdot \widehat{\mathbf{v}} - u(\rho, s) \right) \mathbf{dr} \tag{2.3}$$

where $\widehat{\mathbf{v}}$ is a smoothed velocity. The argument for replacing the kinetic energy term $\frac{1}{2}\mathbf{v}\cdot\mathbf{v}$ by $\frac{1}{2}\widehat{\mathbf{v}}\cdot\mathbf{v}$ is to ensure the Kelvin circulation theorem is still true for the modified equations of motion [28].

The SPH equivalent is

$$L = \sum_b m_b \left( \frac{1}{2} \mathbf{v}_b \cdot \widehat{\mathbf{v}}_b - u(\rho_b, s_b) \right), \tag{2.4}$$

and this choice can be justified because it ensures that the discrete Kelvin circulation theorem is recovered (see Section 3).

The invariant energy (in the absence of viscous dissipation and external or boundary forces) is

$$E = \sum_b m_b \left( \frac{1}{2} \mathbf{v}_b \cdot \widehat{\mathbf{v}}_b + u(\rho_b, s_b) \right). \tag{2.5}$$

The typical LANS model uses a smoothed velocity $\widehat{\mathbf{v}}$ defined in terms of the disordered velocity $\mathbf{v}$ by

$$\widehat{\mathbf{v}}(\mathbf{r}) = \int \mathbf{v}(\mathbf{r}') G(|\mathbf{r}' - \mathbf{r}|, \ell) \mathbf{dr}', \tag{2.6}$$

where the integration is over the region occupied by the fluid, and $G$ is a kernel which satisfies

$$\int G(|\mathbf{r}' - \mathbf{r}|, \ell) \mathbf{dr}' = 1, \tag{2.7}$$

and is a member of a sequence of functions which tends to the $\delta$ function in the limit where $\ell \to 0$. A typical example is a Gaussian, though in this paper we use smooth functions that have compact support. The length scale $\ell$ determines the characteristic width of the kernel and the distance over which the velocity is smoothed. The smoothed velocity defined by (2.6) is identical to that in Large Eddy Simulation. If $G(|\mathbf{q}|, \ell)$ is the Green's function of the Helmholtz equation the following equation

$$\ell^2 \nabla^2 \widehat{\mathbf{v}} = \widehat{\mathbf{v}} - \mathbf{v}, \tag{2.8}$$

can be derived from (2.6). In the LANS-alpha formalism $\ell$ is replaced by $\alpha$. It is common practice (e.g. [8,9,14]) to use this differential equation for the smoothing rather than the integral form (2.6). One reason is that, in three dimensions, the kernel giving the Helmholtz equation is

$$G(|\mathbf{q}|, \ell) = \frac{\mathrm{e}^{-q/\ell}}{4\pi \ell^2 q}, \tag{2.9}$$

and an integration of this function with an accuracy of 1% requires a domain with $0 \le q \ge 7\ell$. Since this integral must be evaluated for each point, the computational cost is very high.

If $\widehat{\mathbf{v}}$ and $\mathbf{v}$ can be expanded in a Fourier series (which we assume to be the case throughout this section) with coefficients of the Fourier term $\mathrm{e}^{\mathrm{i}\mathbf{k}\cdot\mathbf{r}}$, $\widehat{C}_k$ and $C_k$ respectively, then Eq. (2.6) gives

$$\widehat{C}_k = \widetilde{G}(k) C_k, \tag{2.10}$$

where $\widetilde{G}(k)$ is the Fourier transform of $G$ defined by

$$\widetilde{G}(k) = \int \mathrm{e}^{\mathrm{i}\mathbf{k}\cdot\mathbf{r}} |G(|\mathbf{r}|, \ell) \mathbf{dr}. \tag{2.11}$$

Because of (2.7), $\tilde{G}(0) = 1$, and because $G$ is a function of $|\mathbf{r}|$, $\tilde{G}(k) \le 1$. If $G$ is a smooth enough function the Fourier transform decreases rapidly with increasing $k$ so that $\widehat{C}_k \ll C_k$. The smoothing Eq. (2.8) behaves similarly and leads to

$$\widehat{C}_k = \frac{C_k}{1 + \ell^2 k^2}. \tag{2.12}$$

A disadvantage with (2.8), and with the smoothing discussed by Monaghan [29] for a preliminary form of SPH turbulence, is that it can only be solved by iteration when the domain is complicated. In three dimensions the large number of iterations required may then make the implicit smoothing impracticable. The implicit SPH smoothing [29] was too slow even for two-dimensional problems because of the large number of iterations required, and the implicit smoothing (2.7) greatly increases the computational time of LANS-$\alpha$ ocean models [30]. We therefore consider a different smoothing which can be converted to the SPH formulation easily, and involves negligible extra work compared with a standard non-turbulent SPH model. Furthermore we require that the smoothing will conserve linear and angular momentum when it should. The smoothing is the XSPH smoothing [31]

$$\widehat{\mathbf{v}}(\mathbf{r}) = \mathbf{v}(\mathbf{r}) + \epsilon \int (\mathbf{v}(\mathbf{r}') - \mathbf{v}(\mathbf{r})) G(|\mathbf{r}' - \mathbf{r}|, \ell) \mathbf{dr}'. \tag{2.13}$$

The parameter $\epsilon$ is a constant which can be related to $\alpha$ by expanding the term $(\mathbf{v}(\mathbf{r}') - \mathbf{v}(\mathbf{r}))$ in a Taylor series up to quadratic terms. The resulting approximation is identical to (2.8) with $\alpha = h\sqrt{\epsilon g/d}$, where $d$ is the number of dimensions and $g$ is $\int (r/h)^2 W \mathbf{dr}$.

The smoothing occurs for length scales $\lesssim \ell$, and the magnitude of the smoothing is determined by $\epsilon$ and $\ell$. We refer to the SPH turbulence model using this smoothing as the SPH-$\epsilon$ turbulence model.

The Fourier coefficients of the velocities satisfy

$$\widehat{C}_k = C_k(1 + \epsilon(\widetilde{G}(k) - 1)), \tag{2.14}$$

and $\widehat{C}_k \to (1-\epsilon)C_k$ as $k \to \infty$. Provided $|1-\epsilon|$ is sufficiently small $\widehat{C}_k \ll C_k$ as $k \to \infty$. The smoothed velocity spectrum for large $k$ therefore retains the *same form* as the unsmoothed spectrum, though it is reduced in magnitude. The standard LANS-$\alpha$ model changes the spectrum for high $k$ as in (2.12). In the calculations we describe in this paper, where typically $\epsilon$ is 0.8, the high order Fourier coefficients are reduced by a factor 0.2 every step.

The effect of the smoothing on the kinetic energy can be seen by applying (2.14) to the continuum form of the kinetic energy, namely

$$E_K = \frac{1}{2}\int \rho \mathbf{v}\cdot\widehat{\mathbf{v}}\mathbf{dr}, \tag{2.15}$$

and, assuming the density $\rho$ is constant, we get

$$E_K = \frac{1}{2}\rho \sum_k |C_k|^2(1 - \epsilon + \epsilon\tilde{G}(k)) \tag{2.16}$$

which shows that $E_K \geq 0$ if $0 < \epsilon \leq 1$ and $\tilde{G}(k)$ is positive definite. Note that $E_K$ calculated with $\mathbf{v}\cdot\widehat{\mathbf{v}}$ is less than $E_K$ calculated using $\mathbf{v}\cdot\mathbf{v}$.

Applying the SPH procedure for evaluating integrals using information at the particles (see for example the review [1]) the smoothed velocity for particle $a$ can be written

$$\widehat{\mathbf{v}}_a = \mathbf{v}_a + \epsilon \sum_b \frac{m_b}{M}(\mathbf{v}_b - \mathbf{v}_a)K_{ab}, \tag{2.17}$$

where we make the replacement

$$\frac{G(|\mathbf{r}_a - \mathbf{r}_b|, \ell_{ab})}{\rho_b} \to \frac{K_{ab}}{M}. \tag{2.18}$$

The dimensionless function $K_{ab}$ denotes $K(|\mathbf{r}_a - \mathbf{r}_b|, \ell_{ab})$ and $K_{ab} = K_{ba}$. We denote a symmetric average of $\ell_a$ and $\ell_b$ by $\ell_{ab}$ which in this paper we choose to be $\frac{1}{2}(\ell_a + \ell_b)$. $M$ is a mass. In a nearly incompressible $d$-dimensional SPH fluid, where the particles have equal mass $m = \rho_0(dp)^d$, the initial particle spacing is $dp$ and $\rho_o$ is the initial density, $M$ can be taken as $\rho_0\ell^d$. From (2.17) the following chain of equalities holds

$$\begin{aligned}\frac{\mathrm{d}}{\mathrm{d}t}\sum_a m_a\mathbf{r}_a &= \sum_a m_a\frac{\mathrm{d}\mathbf{r}_a}{\mathrm{d}t} = \sum_a m_a\widehat{\mathbf{v}}_a \\ &= \sum_a m_a\mathbf{v}_a = \mathcal{P},\end{aligned} \tag{2.19}$$

where $\mathcal{P}$ is the momentum which is conserved for the set of equations we derive below. In the absence of external forces and fixed boundaries the angular momentum is also conserved because $\sum_a m_a\widehat{\mathbf{v}}_a \times \mathbf{v}_a = 0$, and then

$$\begin{aligned}\frac{\mathrm{d}}{\mathrm{d}t}\sum_a m_a\mathbf{r}_a\times\mathbf{v}_a &= \sum_a m_a\left(\widehat{\mathbf{v}}_a\times\mathbf{v}_a + \mathbf{r}_a\times\frac{\mathrm{d}\mathbf{v}_a}{\mathrm{d}t}\right) \\ &= \sum_a m_a\mathbf{r}_a\times\frac{\mathrm{d}\mathbf{v}_a}{\mathrm{d}t} = 0,\end{aligned} \tag{2.20}$$

where the last equality follows from the invariance properties of the SPH-$\epsilon$ equations (see below).

## 3. Lagrange's equations

Lagrange's equations for particle $c$ are

$$\frac{\mathrm{d}}{\mathrm{d}t}\left(\frac{\partial L}{\partial\widehat{\mathbf{v}}_c}\right) = \frac{\partial L}{\partial\mathbf{r}_c}. \tag{3.1}$$

The Lagrangian must therefore be written in terms of the $\widehat{\mathbf{v}}$ and $\mathbf{r}$. The resulting equations are straightforward to analyze, but the details are lengthy and can be found in the Appendix. The final result is the following very simple equation for the acceleration of any particle $c$

$$\begin{aligned}\frac{\mathrm{d}\mathbf{v}_c}{\mathrm{d}t} &= -\sum_b m_b\left(\frac{P_c}{\rho_c^2} + \frac{P_b}{\rho_b^2}\right)\nabla_c W_{cb} \\ &\quad + \frac{\epsilon}{2}\sum_b \frac{m_b}{M}|\mathbf{v}_c - \mathbf{v}_b|^2\nabla_c K_{cb}.\end{aligned} \tag{3.2}$$

The continuum equivalent of (3.2) is the following Euler equation with an extra term due to the smoothing

$$\begin{aligned}\frac{\partial\mathbf{v}}{\partial t} + (\widehat{\mathbf{v}}\cdot\nabla)\mathbf{v} &= -\frac{1}{\rho}\nabla P \\ &\quad + \frac{\epsilon}{2M}\int \rho\left|\mathbf{v}(\mathbf{r}) - \mathbf{v}(\mathbf{r}')\right|^2\nabla K(\mathbf{r}-\mathbf{r}', \ell)\mathbf{dr}'.\end{aligned} \tag{3.3}$$

If the last term is approximated by expanding the velocity difference in a Taylor series and integrating by parts to remove the derivative of $K$, the $x$ component can be written

$$\begin{aligned}&\frac{\epsilon\mathcal{F}\rho}{2M}\left(\frac{\partial v^x}{\partial x}\nabla^2 v^x + \frac{\partial v^y}{\partial y}\nabla^2 v^y\right. \\ &\quad \left. + \frac{\partial}{\partial x}\left[\nabla v^x\cdot\nabla v^x + \nabla v^y\cdot\nabla v^y\right]\right)\end{aligned} \tag{3.4}$$

where

$$\mathcal{F} = \int (x-x')^2 K\mathbf{dr}' = \int (y-y')^2 K\mathbf{dr}' = \sigma\ell^4, \tag{3.5}$$

$\sigma$ is a non-dimensional constant which depends on the smoothing kernel. We have assumed that $\nabla\cdot\mathbf{v} = 0$, and the point $\mathbf{r}$ is sufficiently far from the boundaries that the integrations can be extended over the entire domain for which $K$ is non-zero. This term involving $\epsilon$ is the equivalent of the derivative of the turbulence stress tensor in LES models of turbulence, and has the same structure as the velocity derivative terms in the LANS-alpha equations [6].

The SPH-$\epsilon$ acceleration equation (3.2) is Galilean invariant, and invariant to a rotation of the coordinate system. For these reasons the linear and angular momentum are conserved. Because the Lagrangian is not an explicit function of time the energy (2.5) is also conserved. The discrete time stepping equations also conserve linear momentum and angular momentum to within round off errors, but the conservation of energy depends on the time stepping algorithm. As discussed in Section 3.3 the time stepping we use is based on the Verlet symplectic integrator and with a standard CFL time step rule, the energy in a non-dissipative system is typically conserved with a relative error of 0.01%. The convergence rule for the iterations is that the relative error is $10^{-6}$.

The equations also satisfy a discrete version of Kelvin's circulation theorem (this follows from the same argument used by Monaghan [1]). This argument is the following. Consider a set of SPH particles which form a closed loop (think of this as a necklace with the beads replaced by particles). If each particle $j$ on the necklace is moved to the position of its neighbor $(j+1)$ on the necklace and, at the same time, its velocities $\mathbf{v}_j$ and $\widehat{\mathbf{v}}_j$ are change to those of $(j+1)$,

the system is unchanged except for a label change. According to Noether's theorem the Lagrangian is unchanged. Therefore

$$\delta L = \sum_j \left( \frac{\partial L}{\partial \mathbf{r}_j} \cdot \delta \mathbf{r}_j + \frac{\partial L}{\partial \widehat{\mathbf{v}}} \cdot \delta \widehat{\mathbf{v}}_j \right), \tag{3.6}$$

where the summation is over all particles forming the necklace. From Lagrange's equations, and noting $\delta \mathbf{r}_j = \mathbf{r}_{j+1} - \mathbf{r}_j$, and $\delta \widehat{\mathbf{v}}_j = \widehat{\mathbf{v}}_{j+1} - \widehat{\mathbf{v}}_j$, we can write the previous expression as

$$\delta L = \frac{\mathrm{d}}{\mathrm{d}t} \left( \sum_j \frac{\partial L}{\partial \widehat{\mathbf{v}}_j} \cdot \delta \mathbf{r}_j \right) = 0. \tag{3.7}$$

We show in the Appendix that the canonical momentum for a particle $c$, namely $\partial L/\partial \widehat{\mathbf{v}}_c$, is $m_c \mathbf{v}_c$. Assuming all particles have the same mass, we deduce that the discrete circulation

$$C = \sum_j \mathbf{v}_j \cdot \delta \mathbf{r}_j \sim \oint \mathbf{v} \cdot \mathbf{dr}, \tag{3.8}$$

is constant. This result is only true if the kinetic energy in the Lagrangian takes the form $\frac{1}{2}\widehat{\mathbf{v}} \cdot \mathbf{v}$, and provides a justification for our choice of the kinetic energy, as in the argument given by Foias et al. [28].

This invariant is, however, only approximate because Noether's theorem assumes the transformations are infinitesimal whereas the transformations described above are discrete. The approximation is better as the particle spacing becomes smaller relative to the length scale of the velocity variations. If the shift of the particles on the necklace is in the opposite direction, the invariant can be obtained with the opposite sign. Combining this with the previous result, and taking account of the signs, we can write the discrete circulation in the form

$$C = \frac{1}{2} \sum_j \mathbf{v}_j \cdot (\mathbf{r}_{j+1} - \mathbf{r}_{j-1}). \tag{3.9}$$

In this paper we choose the kernels $G$ and $W$ to be identical and the function $K = G\ell^d$. For our two-dimensional calculations $W$ is the 2D Wendland function [32], apart from a different scaling. This function is

$$G(z, \ell) = \frac{7}{64\pi \ell^2}(2 - z/\ell)^4(1 + 2z/\ell), \tag{3.10}$$

if $z \le 2\ell$, and zero otherwise. Numerical integrations of the Fourier transform of this function shows that it decreases monotonically as $k$ increases. The Fourier transform of the Cubic Spline kernel, which is often used in SPH calculations, has sharp rises and falls for $k\ell > 2\pi$.

For the two-dimensional calculations we choose $\ell$ to be $h$ and $M = \rho_0 \ell^2$ where $\rho_0$ is the initial density. In that case we can replace (3.2) by

$$\frac{\mathrm{d}\mathbf{v}_c}{\mathrm{d}t} = -\sum_b m_b \left( \frac{P_c}{\rho_c^2} + \frac{P_b}{\rho_b^2} - \frac{\epsilon}{2} \frac{|\mathbf{v}_c - \mathbf{v}_b|^2}{\rho_0} \right) \nabla_c W_{cb}. \tag{3.11}$$

### 3.1. Pressure and viscosity

In this paper we assume the fluid is weakly compressible. The equation of state can be taken as

$$P = \frac{\rho_0 c_s^2}{\gamma} \left( \left( \frac{\rho}{\rho_0} \right)^\gamma - 1 \right), \tag{3.12}$$

where $\rho_0$ is a reference density, $c_s$ is the speed of sound, and $\gamma = 7$ in this paper. For the weakly compressible case we choose $c_s = 10 V_{\max}$ where $V_{\max}$ is the maximum fluid velocity, so that the relative density fluctuation $\delta\rho/\rho \sim (v_{\max}/c_s)^2 = 0.01$.

To complete our model we need to add a viscous term. There are several SPH approximations to the Navier–Stokes viscosity (see [1] for two examples). The viscous equations take the form

$$\frac{\mathrm{d}\mathbf{v}_c}{\mathrm{d}t} = -\sum_b m_b \left( \frac{P_c}{\rho_c^2} + \frac{P_b}{\rho_b^2} + \Pi_{bc} - \frac{\epsilon}{2} \frac{|\mathbf{v}_{bc}|^2}{\rho_0} \right) \nabla_c W_{cb} \tag{3.13}$$

where the viscosity term $\Pi_{bc}$ is defined by

$$\Pi_{bc} = -\frac{\alpha v_{sig} \mathbf{v}_{bc} \cdot \mathbf{r}_{bc}}{\bar{\rho}_{bc} r_{bc}}, \tag{3.14}$$

and for any vector $\mathbf{k}$ we have replaced $(\mathbf{k}_b - \mathbf{k}_c)$ by $\mathbf{k}_{bc}$. In this expression $\alpha$ is a constant (we retain the standard SPH notation but refer to it as the viscous $\alpha$), $v_{sig}$ is a signal velocity which, in this paper, is taken as the speed of sound in the equation of state, and $\bar{\rho}_{bc} = (\rho_b + \rho_c)/2$. If the density is constant, and the kernel $W$ is a Wendland fourth order kernel, it is possible to show by converting the SPH summations into integrals [1] that the kinematic viscosity $\nu$ is

$$\nu = \frac{1}{8} \alpha c_s h. \tag{3.15}$$

### 3.2. Boundaries and boundary forces

In this paper the boundaries are defined by boundary particles which exert forces on the fluid. The boundaries can be external or internal. The technique is similar to the immersed boundary method of Peskin (1977, 2002), [18,19] and is discussed in detail by Monaghan and Kajtar [17]. The basic idea is that if the force between a fluid and a boundary particle is a sufficiently smooth function of their separation, and along their line of centers, the force on a fluid particle is normal to the boundary with high accuracy. Monaghan and Kajtar [17] showed that this is true for both curved and planar surfaces.

When the boundary force particles are included the acceleration of a fluid particle $c$ becomes

$$\frac{\mathrm{d}\mathbf{v}_c}{\mathrm{d}t} = -\sum_b m_b \left( \frac{P_c}{\rho_c^2} + \frac{P_b}{\rho_b^2} - \frac{\epsilon}{2} \frac{v_{bc}^2}{\widetilde{\rho}_{bc}} + \Pi_{bc} \right) \nabla_c W_{cb} + \sum_{k=1}^{N_b} \sum_{j \in S_k} m_j \left( \mathbf{f}_{cj} - \Pi_{jc} \nabla_c W_{jc} \right), \tag{3.16}$$

where the sum over $k$ is over the $N_b$ bodies which may be external boundaries or the boundaries of bodies moving in the fluid. $j \in S_k$ denotes the boundary particles of body $k$.

In this paper we use the following form for the force per unit mass $\mathbf{f}_{cj}$ on fluid particle $c$ by boundary particle $j$

$$\mathbf{f}_{cj} = \frac{0.01 c_s^2 B(r_{cj})}{(|r_{cj} - \Delta|)} \frac{\mathbf{r}_{cj}}{r_{cj}}, \tag{3.17}$$

where $B(r)$ is the one-dimensional cubic Wendland function [32] which has been scaled so that it is only non-zero in the domain $0 < r/h < 2$ where it has the form

$$\frac{1}{16} \left( 2 + 3\frac{r}{h} \right) \left( 2 - \frac{r}{h} \right)^3. \tag{3.18}$$

The parameter $\Delta$ is the spacing of the boundary force particles. Provided $\Delta$ is less than $0.5dp$, where $dp$ is the typical fluid particle spacing, the tangential component of the force is $<10^{-5}$ of the normal component. Further details can be found in the paper by Monaghan and Kajtar [17]. Because the boundary force between a

pair of particles is radial it is possible to write it in terms of a pair potential which can then be included in the Lagrangian.

The present formulation is general and allows for an arbitrary number of boundaries of arbitrary shape. These bodies may move either by specifying their motion or by determining it from the forces exerted on the boundary force particles by the fluid particles. In this paper the only boundary is the fixed square boundary containing the fluid.

### 3.3. Time stepping

The SPH turbulence equations were integrated using a time stepping scheme that is second order and based on the Verlet symplectic method. The ideal form is reversible in the absence of viscosity. Other higher order symplectic schemes could be used, or methods based on discrete mechanics and variational principles as proposed by Marsden and West [33]. However, the Verlet symplectic integrator is simple and efficient.

For convenience we write the equation in the form

$$\frac{\mathrm{d}\mathbf{v}_c}{\mathrm{d}t} = \mathbf{F}(\mathbf{r}, \rho, \mathbf{v})_c, \tag{3.19}$$

$$\frac{\mathrm{d}\rho_c}{\mathrm{d}t} = Q(\mathbf{r}, \widehat{\mathbf{v}}), \tag{3.20}$$

$$\frac{\mathrm{d}\mathbf{r}_c}{\mathrm{d}t} = \widehat{\mathbf{v}}_c, \tag{3.21}$$

$$\widehat{\mathbf{v}}_c = \mathbf{g}(\mathbf{v}_c, \mathbf{r}_c). \tag{3.22}$$

In the following $A^0$ denotes a quantity $A$ at the beginning of the current step, $A^{1/2}$ at the midpoint of the step, and $A^1$ at the end of the step. With $\delta t$ the time step, $\mathbf{r}_c$ and $\rho_c$ can be integrated half a step

$$\mathbf{r}_c^{1/2} = \mathbf{r}_c^0 + \frac{1}{2}\delta t\widehat{\mathbf{v}}^0, \tag{3.23}$$

$$\rho_c^{1/2} = \rho_c^0 + \frac{1}{2}\delta t Q_c^0, \tag{3.24}$$

then $\mathbf{v}_c^1$ is calculated from

$$\mathbf{v}_c^1 = \mathbf{v}_c^0 + \delta t\mathbf{F}_c(\mathbf{r}^{1/2}, \rho^{1/2}, (\mathbf{v}^1 + \mathbf{v}^{\mathbf{0}})/2), \tag{3.25}$$

after which $\widehat{\mathbf{v}}^1$, $\mathbf{r}^1$ and $\rho^1$ can be calculated according to

$$\widehat{\mathbf{v}}^1 = \mathbf{g}(\mathbf{v}^1, \mathbf{r}^1), \tag{3.26}$$

$$\mathbf{r}_c^1 = \mathbf{r}_c^{1/2} + \frac{1}{2}\delta t\widehat{\mathbf{v}}_c^1, \tag{3.27}$$

$$\rho_c^1 = \rho_c^{1/2} + \frac{1}{2}\delta t Q_c^1. \tag{3.28}$$

This algorithm is reversible in the absence of dissipation, and it conserves linear and angular momentum to within round off errors. Because iteration is required to solve (3.25) we compromise in the interest of faster computation by replacing $(\mathbf{v}_c^1 + \mathbf{v}_c^0)/2$ with $\mathbf{v}_c^{1/2}$ and estimate $\mathbf{v}_c^{1/2}$ by

$$\mathbf{v}_c^{1/2} = \mathbf{v}_c^0 + \frac{1}{2}\delta t\mathbf{F}_c^{-1/2}, \tag{3.29}$$

which introduces errors $O(\delta t)^2$ in $\mathbf{v}_c^{1/2}$ and therefore errors of $O(\delta t)^3$ in $\mathbf{v}_c^1$. This does not affect the conservation of linear and angular momentum. The two Eqs. (3.26) and (3.27) also require iteration. Clearly the number of iterations depends on the time step and $\epsilon$ and, if either is too large, the iterations will not converge. The condition on the time step to guarantee the iteration will converge is easily worked out. However, for all the calculations in this paper where $0 < \epsilon < 0.9$, the iterations converge in 3 steps with an error of $10^{-6}$ with just the CFL condition $\delta t < 0.5h/c_s$. Note that the function $\mathbf{g}(\mathbf{v}, \mathbf{r})$ also contains $\ell$ or, in the present case, $h$. When iterating (3.26) and (3.27) this is replaced by the midpoint value calculated using the midpoint density.

## 4. Applications to turbulence in a square 2D rigid box

We consider a two-dimensional fluid inside a square boundary. We use SI units throughout. The side length of the square boundary is 1 m and boundary conditions no-slip. This problem provides a good test of turbulence models because it has been studied in great detail by laboratory experiment, and by highly accurate numerical simulations (see for example [21,22,24]). Furthermore, the computer time is greatly reduced relative to three dimensions and the calculations described here were run on a MacBook Pro. The results of [21] which we use for comparison, have Reynolds numbers $\Re$ in the range 1000–5000. In this range their results for the decay of the kinetic energy and the enstrophy, and the vortex formation are similar.

For the SPH simulation we use the 4th order Wendland kernel $W(r, h)$ identical to $G$ defined by (3.23). The initial particle density was $1.01\rho_w$ where $\rho_w$ is the density of water, and the reference density for the equation of state. This produces a small background pressure. The smoothing length $h$ was set to $1.5dp$ where $dp$ is the particle spacing. The smoothing of the velocity is therefore over a circle of radius $\sim 3dp$ around any specified particle.

The Reynolds number $\Re$, with velocity 0.12 m/s (which is the typical maximum velocity in the box after the few seconds), and length scale equal to half the side of the box, was 1000. This $\Re$ is similar to those used by Clercx et al. [21] who considered $\Re$ in the range $500 < \Re < 2000$. With the $\Re$ specified, and the kinematic viscosity given by (3.15), the value of the viscous $\alpha$ for a specified resolution, and therefore specified $h$, can be calculated. The resolution length for a well resolved calculation can be estimated in the same way as did [21] from the enstrophy dissipation rate giving an estimate of the resolution length required for a DNS simulation in a box of side 1 as $\sim 1/\sqrt{\Re}$. They found that for their box of side 2 they required a resolution length of 2/180. We find that convergence is achieved for an SPH calculation with a resolution of 1/150.

The SPH particles were placed initially on a grid of squares then damped to equilibrium, after which they were set in motion with velocities specified by a $4 \times 4$ set of vortices. A similar procedure was used by Maassen et al. [24] though they had higher resolution and used a $10 \times 10$ set of Gaussian vortices. The vortices for the present simulations were initially equi-spaced, with spacing 0.2, then given a random shift in both $x$ and $y$ of $0.02\eta$ where $\eta$ is a uniformly distributed random number with $-1 < \eta < 1$. The sign of the rotation and hence vorticity due to each vortex was $\pm$ in a chess board pattern. The velocity at $\mathbf{r}$ due to a vortex at $\mathbf{R}$ is

$$\mathbf{v}(\mathbf{r}) = \Omega\mathbf{e}_z \times (\mathbf{r} - \mathbf{R}), \tag{4.1}$$

where $\mathbf{e}_z$ is a unit vector normal to the fluid and $\Omega$ is given by

$$\Omega = \frac{d}{2\pi|\mathbf{r} - \mathbf{R}|^2}\left(1 - \mathrm{e}^{-(|\mathbf{r}-\mathbf{R}|^2/d^2)}\right), \tag{4.2}$$

and $d = 0.02$.

The Fourier transform of the vorticity produced by this velocity field decreases exponentially according to $\mathrm{e}^{-(kd/2)^2}$. The no-slip condition requires that the fluid velocity vanishes on the boundary. This was achieved by smoothing the velocity near the boundaries in a similar manner to [22]. The mean square speed was initially 0.15 m/s giving a typical time scale of $1.0/0.15 \sim 6$ s.

In Fig. 1 we show the smoothed velocity field of a set of fluid particles with $\epsilon = 0.9$ and initial spacing 1/75 at a time 5 s (or $\sim 1$

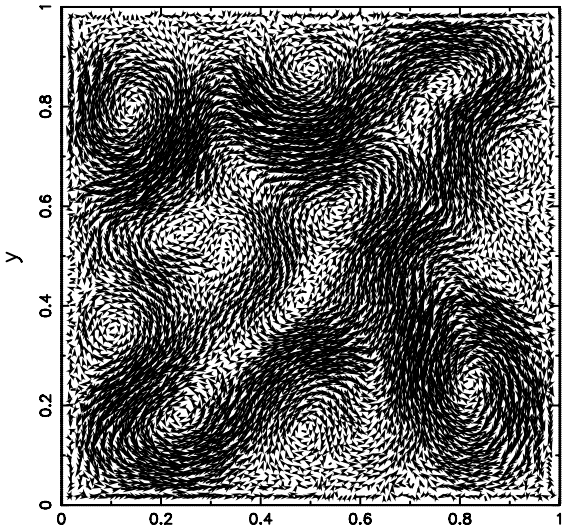


**Fig. 1.** The $\widehat{\mathbf{v}}$ field for $\epsilon = 0.9$ shown after 5 s (approximately a turnover time). The small length scale structures have been replaced by larger scales.

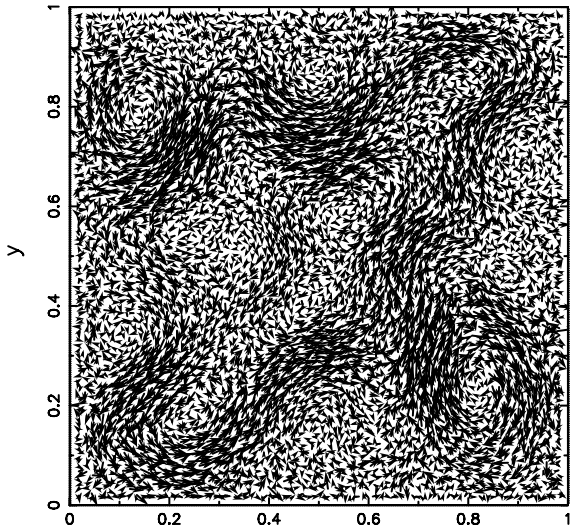


**Fig. 2.** The unsmoothed velocity field $\mathbf{v}$ field for $\epsilon = 0.9$ shown after 5 s (approximately a turnover time). Comparison with the smoothed velocity of the previous figure shows that the smoothing removes the short length scales.

time scale) after damping. Fig. 2 shows the unsmoothed velocity field at the same time. A comparison of these two figures shows that the small scale disorder of the unsmoothed velocity field has been removed by the smoothing process. In Fig. 3 the smoothed velocity field is shown after 15 s (or 3 time scales). Already much of the complex short length scale velocity field has transformed into larger scales which is similar to that found in experiments and in other simulations ([24], their Fig. 3). A similar result was found when the simulation was run without smoothing indicating that the transformation is not due to the smoothing but to the normal processes that occur in two-dimensional turbulence.

### 4.1. Decay of kinetic energy and enstrophy with time

We now consider quantitative results derived from the decay of energy and enstrophy and the form of the second and fourth order velocity correlation functions. The kinetic energy is given by

$$E_K = \frac{1}{2}\sum_a m_a \widehat{\mathbf{v}}_a \cdot \mathbf{v}_a, \tag{4.3}$$

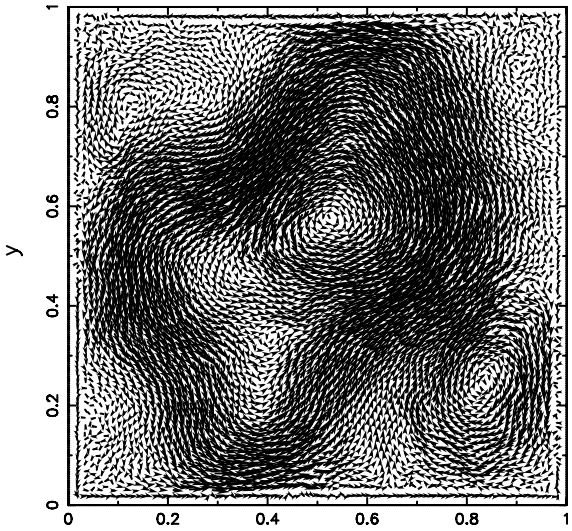


**Fig. 3.** The $\widehat{\mathbf{v}}$ field for $\epsilon = 0.9$ shown after 15 s (3 typical turnover times). The velocity structures now have larger length scale than in Fig. 1.

and the enstrophy $\zeta$ is given by

$$\zeta = \frac{1}{2}\int (\nabla \times \mathbf{v})^2 \mathbf{dr} = \frac{1}{2}\sum_a \frac{m_a}{\rho_a}(\nabla \times \mathbf{v})_a^2. \tag{4.4}$$

The vorticity $\nabla \times \mathbf{v}$ can be calculated in two ways. The first is by using SPH which results in the following expression for the vorticity of particle $a$

$$(\nabla \times \mathbf{v})_a = \sum_b \frac{m_b}{\rho_b}(\mathbf{v}_{ba} \times \mathbf{r}_{ab})F_{ab}, \tag{4.5}$$

where we have written $\nabla_a W_{ab} = \mathbf{r}_{ab}F_{ab}$. Note that this expression involves a term which is the relative angular momentum per unit mass. The second method of calculating the vorticity is to assume the components of the velocity relative to a given particle can be approximated by a linear expansion in the coordinates $x$ and $y$. The constants in the expansions can be calculated by least squares. This gives more accurate results than the first method and we use it here.

While it is common in turbulence simulations to calculate spectra we do not do so here for the following reason. To determine the effect of smoothing it is necessary to calculate the spectral coefficients up to order $1/(3dp)$ because the smoothing is over the distance $3dp$. However, such high order coefficients cannot be calculated accurately either by SPH summation, or by mapping to a grid. In the latter case, for a grid of squares with side $jdp$ where $j$ is 1 or 2, the mapping introduces a smoothing which obscures the smoothing of the turbulence model. By comparison the velocity correlation functions are easy to calculate and show the effects of the turbulence very clearly. For that reason we concentrate our analysis on the correlation functions.

In Fig. 4 we show the decay of kinetic energy $E_K$ (defined as in (3.5)), for three simulations with initial particle spacing 1/100, 1/150 and 1/200 and $\epsilon = 0$. [24] find that the kinetic energy decays with time approximately as $1/t$ for the case of weak stratification (their Fig. 9(a)) which is close to the decay of $1/t^{0.8}$ indicated in Fig. 4. In all cases, provided $t \gtrsim 10$, we find $E_K \sim A/t^{\beta}$ with $\beta \sim 0.8$. More accurate estimates of $\beta$ are given below in the discussion of convergence.

The decay of the enstrophy is shown in Fig. 5 where the line of small open circles has the time variation $1/t^{1.7}$. The results are in good agreement with the results of [24] (their Fig. 9(b)) which show that the enstrophy decays according to $1/t^{1.7}$. A difference between the trends for the kinetic energy and the enstrophy is

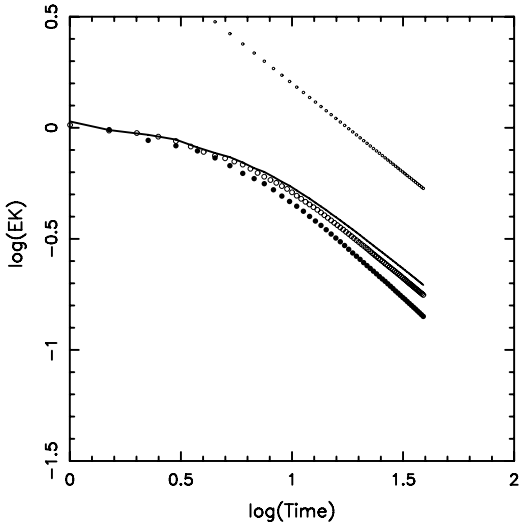


**Fig. 4.** The decay of kinetic energy with time for a simulation with $\epsilon = 0$ is shown. The filled circles are for resolution 1/100, the larger open circle are for resolution 1/150 and the continuous curve for resolution 1/200. The small open circles mark a line with time variation $1/t^{0.8}$.

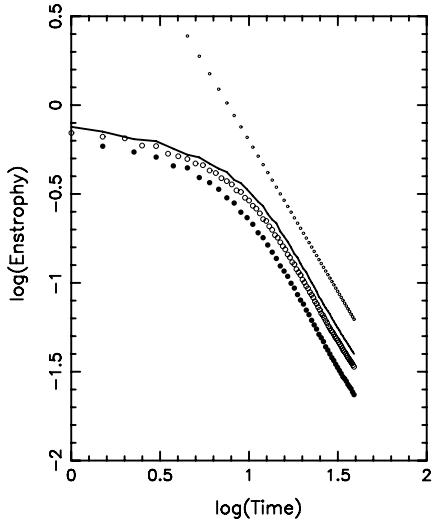


**Fig. 5.** The decay of Enstrophy with time with $\epsilon = 0$. The filled circles are for resolution 1/100, the larger open circle are for resolution 1/150 and the continuous curve for resolution 1/200. The small open circles mark a line with time variation $1/t^{1.7}$.

that in the latter the slopes of the curve for different resolutions are very similar. Provided $t \gtrsim 10$ s, we find the enstrophy varies approximately as $\sim A/t^{\beta}$, as in the case of $E_K$ but $\beta = 1.78$.

In Fig. 6 the time variation of the ratio of enstrophy to kinetic energy is shown. This is also in good agreement with [24] (see their Fig. 17).

#### 4.1.1. Convergence

The convergence of the solution can be found by assuming any quantity $E$ varies with resolution $dp$ according to

$$E(dp) = E(0) + \Gamma(dp)^s. \tag{4.6}$$

By using the values of $E$ for three resolutions the three unknowns $E(0)$, $\Gamma$ and $s$ can be determined. We also calculate the values of $A$ and $\beta$. These are in Table 1.

From the values of $E_K$ we find that $s = 0.81$, $\Gamma = -7.53$ and $E(0) = 0.427$. To check these results the value of $E_K$ at 15 s after damping was calculated for $n_x = 250$. It differed from the estimated $E(0)$ by less than 0.02%. The convergence of $A$ and $\beta$ is close to linear.

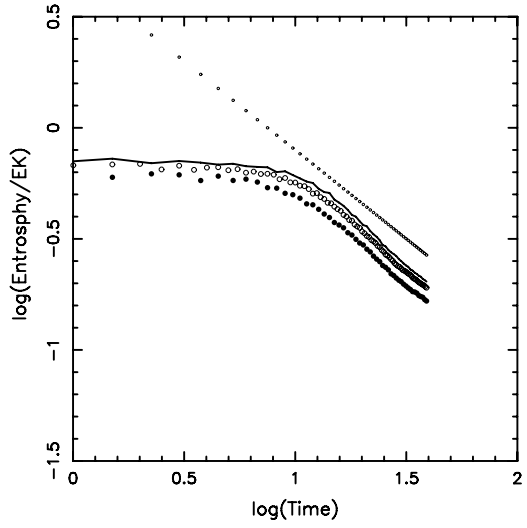


**Fig. 6.** The decay of $Enstrophy/E_K$ with time with $\epsilon = 0$. The filled circles are for resolution 1/100, the larger open circle are for resolution 1/150 and the continuous curve for resolution 1/200. The small open circles mark a line with time variation $1/t^{0.7}$.

**Table 1**
Values of kinetic energy $E_K$ and the parameters $A$ and $\beta$ when $\epsilon = 0$, evaluated 15 s after the damping has ceased.

| $n_x$ | $E_K$ | $A$ | $\beta$ |
|---|---|---|---|
| 100 | 0.332 | 3.60 | 0.88 |
| 150 | 0.383 | 3.17 | 0.78 |
| 200 | 0.410 | 3.02 | 0.74 |

### 4.2. Velocity correlation functions

The $n$th order, longitudinal velocity correlation function $C_n(R)$ for particles separated by the distance $R$ is defined by

$$C_n(R) = \frac{\iint \left[(\mathbf{v}(\mathbf{r}) - \mathbf{v}(\mathbf{r}')) \cdot \mathbf{q}/q\right]^n \delta(q - R)\mathbf{dr}\mathbf{dr}'}{\iint \delta(r - R)\mathbf{dr}\mathbf{dr}'}, \tag{4.7}$$

where $\mathbf{q} = \mathbf{r} - \mathbf{r}'$, $\delta(x)$ denotes a one-dimensional Delta function, and $\mathbf{dr}$ denotes a volume (area in 2D) element. The velocity may be the smoothed or unsmoothed velocity. To see that the expression for $C_n$ is correct it is useful to consider the case where

$$(\mathbf{v}(\mathbf{r}) - \mathbf{v}(\mathbf{r}')) \cdot \mathbf{q}/q = q, \tag{4.8}$$

and assume that the integration is over an area $A$. The integration can then be carried out by using the variables $\mathbf{r}$ and $\mathbf{q}$ instead of $\mathbf{r}$ and $\mathbf{r}'$. We find

$$C_n(R) = \frac{R^n 2\pi AR}{2\pi AR} = R^n, \tag{4.9}$$

as expected.

We evaluate the correlation functions using SPH summations and we replace the $\delta(q - R)$ by the histogram function $H$ defined by $H(q - R) = 1$ if $R - \Delta \le q \le R + \Delta$, otherwise $H(q - R) = 0$. The SPH form of (4.3) is

$$C_n(R) = \frac{\sum_a \sum_b \frac{m_a m_b}{\rho_a \rho_b} (\mathbf{v}_{ab} \cdot \mathbf{r}_{ab}/r_{ab})^n H(r_{ab} - R)}{\sum_a \sum_b \frac{m_a m_b}{\rho_a \rho_b} H(r_{ab} - R)}. \tag{4.10}$$

The most efficient way of evaluating these summations is by binning. We consider every pair of particles. For any two particles

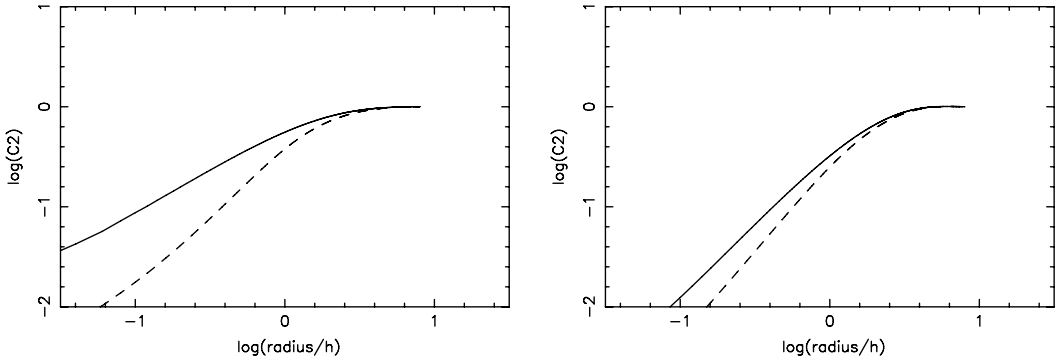


**Fig. 7.** The second order correlation function calculated according to the theory of Babiano et al. [34] with an underlying kinetic energy spectrum $\propto 1/(1+(k/40)^n)$ modified to allow approximately for smoothing. The frame on the left is for $n=2$ and on the right $n=3$. The continuous line shows the results for $\epsilon=0$ and the dashed line the results for $\epsilon=0.9$. Note that the dashed line drops below the continuous line for $r/h\sim 3$.

$a$ and $b$ we calculate an integer $k = \mathrm{Int}(r_{ab}/\Delta)$ where Int is the Fortran integer function and $\Delta$ is a suitable small fraction of the maximum value of $R$. The value of $((\mathbf{v}_a-\mathbf{v}_b)\cdot\mathbf{r}_{ab}/r_{ab})^n$ is added to $F_k$ and 1 is added to $N_k$. The value of $C_n(R_k)$ is then the final value of $F_k/N_k$ where $R_k = k\Delta$. Because the system is not homogeneous or isotropic the correlation function was calculated for points $a$ within the square $0.3 < x < 0.7$, and $0.3 < y < 0.7$, while the points $b$ are those in the entire domain. In this way the influence of the boundary is reduced. In order to make it easier to see the trends of the $C_n$ with resolution it is convenient to divide all values for a given resolution by the maximum value for that resolution.

Before discussing the correlation functions calculated from the SPH simulations it is useful to note the relationship between the correlation functions and the energy spectra derived by Babiano et al. [34] for two-dimensional flow in a doubly periodic domain. They showed that a function $S(r)$, equivalent to $C_2(r)$, is related to the energy spectrum $E(k)$ by

$$S(r) = 4\int_0^\infty \sin^2(kr/2)E(k)\mathrm{d}k. \tag{4.11}$$

Using this expression, which is exact, they consider the variation of $S(r)$ with $r$ when the kinetic energy spectrum varies with wave number $k$ as $k^{-n}$. They evaluate the integral approximately and conclude that if $n < 1$ then $\mathrm{d}S(r)/\mathrm{d}r \sim 0$, if $1 < n < 3$ then $S(r) \sim r^{n-1}$ and if $n > 3$, then $S(r) \sim r^2$. This means that all very steep spectra $n > 3$, for the doubly periodic domain, have similar correlation functions with $S(r) \propto r^2$. In the present case, the results of Clercx and Van Heijst [22] can be approximated by $E(k) \sim 0.1/(1+(k/40)^n)$ where $1.6 < n < 3$. The effect of smoothing can be roughly estimated by replacing this $E(k)$ by the expression

$$E(k) \sim \frac{(1+\epsilon(\widehat{G}(k)-1))}{(1+(k/40)^3)}. \tag{4.12}$$

Substituting this expression into (4.11), and integrating using the variables $kh$ and $r/h$ gives the results shown in Fig. 7 where the continuous line is for $\epsilon = 0.0$ and the dashed line is for $\epsilon = 0.9$. The points to notice are first that the dashed line deviates from the continuous for $r/h \sim 3$ or $r \sim 4.5dp$. The slope of the straight section of the graph is 0.8 for $n=2$ which is approximately that predicted by the theory of Babiano et al. [34] which predicts a slope of $\sim$1. In the case $n$ is 3 and for $n = 4$ (not shown here) the slope is 1.8, which is in approximate agreement with the theory of Babiano et al. [34] that predicts a slope of 2.0. These results suggest that the correlation functions evaluated with $\epsilon$ close to 0.8 can be expected to fall below those with $\epsilon = 0$, and depart from them at a distance of $\sim 4dp$. Of course the actual effects of smoothing are more complicated since they affect the dynamics and lead to an altered velocity field.

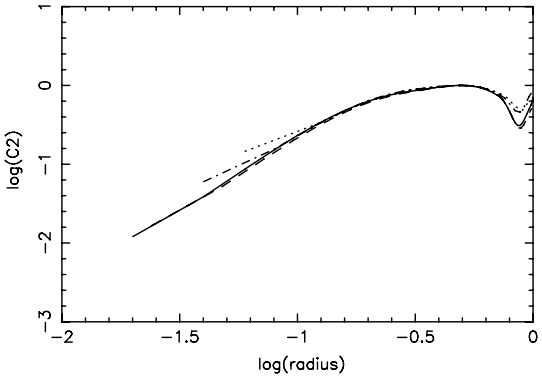


**Fig. 8.** $C_2$ for simulations with $\epsilon = 0$. The continuous line is for initial particle spacing 1/150, the dashed line is for spacing 1/125, the dash–dot line is for spacing 1/75 and the dotted line is for spacing 1/50. Note the change of slope for the spacings 1/50 and 1/75 which begins at separation $\sim 6dp$.

Fig. 8 shows $\log C_2$ against $\log R$ calculated for initial particle spacings 1/50, 1/75, 1/125 and 1/150 for $\epsilon = 0$. For initial spacings 1/150 and 1/125 the slope of the $\log C_2$ curve is close to 2 for $\log R < -0.7$. This is the theoretical slope for the direct cascade in two-dimensional turbulence in a doubly periodic domain where the energy spectrum decays with wave number $k$ according to $k^{-3}$. But, as remarked above, it may also be the slope for any spectrum decaying faster than $k^{-3}$. Theory [35] for homogeneous turbulence in an unbounded domain suggests the energy spectrum should scale as $k^{-5/3}$ for small $R$. The argument of Babiano et al. [34] then leads to $C_2(R) \propto R^{2/3}$. This is approximately true for $-0.7 < \log R < -0.4$.

Fig. 8 and Table 2, show that the slope of the curve of $\log C_2$ against $\log R$, for spacings 1/75 and 1/50, changes from $\sim$2 to $\sim$1.3 for $R \lesssim 6dp$. The physical interpretation of this is that, in this range of $R$, there is much more disorder in the velocity field than theory would predict, and suggested by the simulations with higher resolution. It can also be seen from Fig. 8 that there is also a very slight change in the slope of $C_2$ for the two higher resolution simulations for $R \lesssim 6dp$. The shape of the curves for large values of $R$ reflects the effects of the boundary.

Fig. 9 shows $\log C_4$ calculated for the same initial particle spacings as for $C_2$. The slopes of the curves for spacings 1/150 and 1/125, in the range $-1.5 < \log R < -0.8$ are both close to 4, which is the expected slope for the direct cascade. The slope for spacings 1/75 and 1/50 are close to 2, rather than the expected value of 4, for $\log R < -0.8$ indicating more disorder for this range of $R$. As with $C_2$ there is a very slight change in the slope of $C_4$ for spacings 1/125 and 1/150 for $R \lesssim 6dp$.

**Table 2**
Values of $\lambda$ where $C_n(R) \propto R^{\lambda}$ for the correlation functions $C_2$ and $C_4$ with and without smoothing. The values of $\lambda$ were calculated for the parts of the $\log C_n$, $\log R$ which are close to straight lines.

| | $C_2$ | | $C_4$ | |
|---|---|---|---|---|
| $n_x$ | $\epsilon = 0$ | $\epsilon = 0.8$ | $\epsilon = 0$ | $\epsilon = 0.8$ |
| 50 | 1.2 | 1.3 | 2.2 | 2.4 |
| 75 | 1.3 | 1.7 | 2.5 | 3.3 |
| 150 | 1.9 | 2.0 | 3.5 | 3.9 |

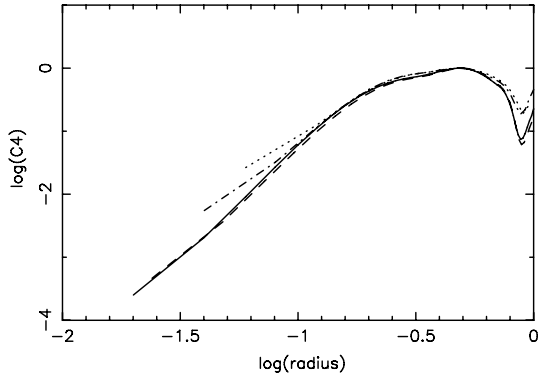


**Fig. 9.** $C_4$ for simulations with $\epsilon = 0$. The notation is the same as for Fig. 7. Note the change of slope for the spacings 1/50 and 1/75 which begins at separation $\sim 6dp$.

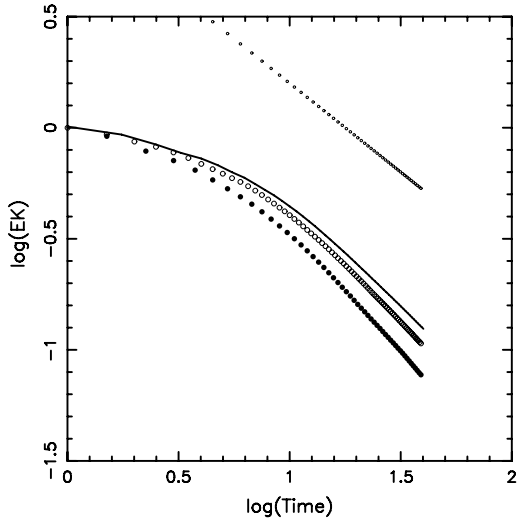


**Fig. 10.** The decay of the kinetic energy for initial spacing 1/100 (filled circles), and 1/150 (large open circles) and 1/200 (continuous line), with $\epsilon = 0.8$. The line of small open circles marks $1/t^{0.8}$.

## 5. The effects of smoothing

We now consider the effects of smoothing on the decay of the kinetic energy and the enstrophy, and the velocity correlation functions.

### 5.1. Energy and enstrophy

We now explore the effects of the turbulence model on the dynamics of the fluid. Fig. 10 shows the decay of $E_K$ (defined by (4.3)). The trends are similar to the case $\epsilon = 0$. In particular $E_K = A/t^{\beta}$ for $t \gtrsim 10$. However, the exponent when $\epsilon = 0.8$ is $\beta \sim 1.0$, whereas for $\epsilon = 0$ it was 0.8. However, as before, the values of the kinetic energy for spacing 1/100 are significantly below those for spacing 1/150. These results show that the turbulence model can reproduce the trends with coarser resolution, but the absolute values may have a significant error. In Fig. 11 the enstrophy is shown when $\epsilon = 0.8$. This also is similar to the case with $\epsilon = 0$. In particular, provided $t \gtrsim 10$ s, we find the enstrophy varies approximately as $\sim A/t^{\beta}$, with $\beta = 1.88$. This value of $\beta$ is larger than the value for $\epsilon = 0$ which was 1.78.

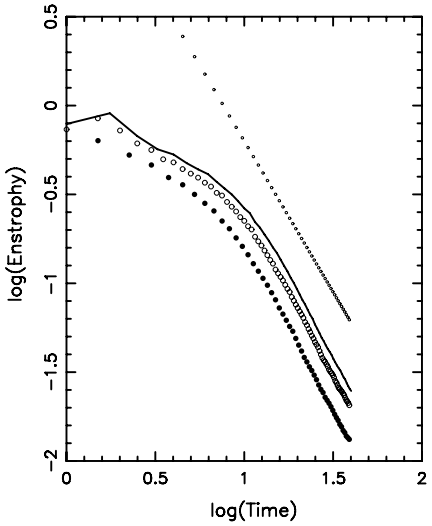


**Fig. 11.** The decay of the enstrophy for initial spacing 1/100 (filled circles), and 1/150 (large open circles) and 1/200 continuous line, with $\epsilon = 0.8$. The line of small open circles marks $1/t^{1.7}$.

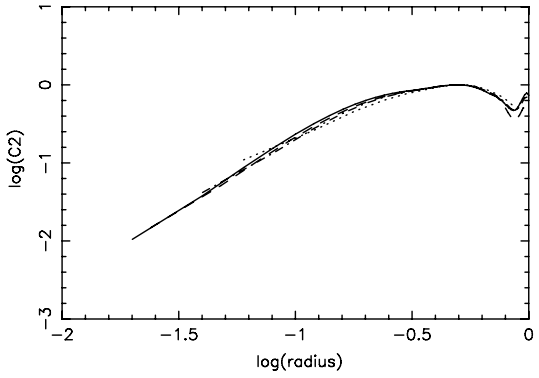


**Fig. 12.** $C_2$ for $\epsilon = 0.8$. The notation is the same as for Fig. 7. The dash–dot curve for spacing 1/75 is now very close to that for spacing 1/150.

### 5.2. Velocity correlation functions with smoothing

In Fig. 12 we show $C_2$ for the case $\epsilon = 0.8$. The notation is the same as for Fig. 7. The key feature of these graphs is that $C_2$ for resolution 1/75 is now very close to that for 1/150 and 1/125, and $C_2$ for resolution 1/50 is now much improved over the results with $\epsilon = 0$. The details of the slopes are given in Table 2. These results indicate that the disorder at short length scales has been reduced. The slope of $C_2$ for resolution 1/150 is close to 2.0, and the very slight change in slope of $C_2$ for $R \lesssim 6dp$ which can be seen in Fig. 7 has now nearly disappeared. These changes are consistent with those in Fig. 7 which show the effect of smoothing appears for $R < 4.5dp$. In Fig. 13 we show $C_4$ for $\epsilon = 0.8$. As with $C_2$ comparison with the results for $\epsilon = 0$ shows that the turbulence model brings the correlation function for resolution 1/75 close to those for resolution 1/125 and 1/150. The very slight change in slope of $C_4$ for $R \lesssim 6dp$ which can be seen in Fig. 9 has now nearly disappeared. The slope of $C_4$ for resolution 1/150 is 3.6. Further details are given in Table 2.

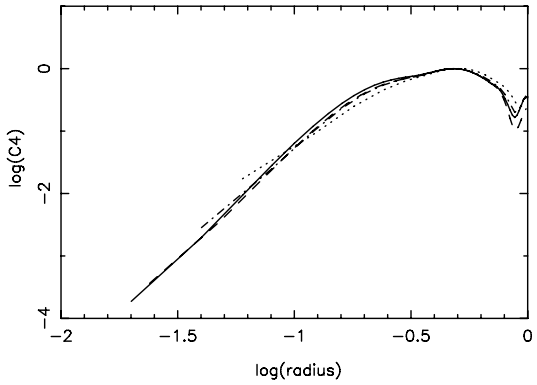


**Fig. 13.** $C_4$ for $\epsilon = 0.8$. The notation is the same as for Fig. 7. The dash–dot curve for spacing 1/75 is now much closer to that for spacing 1/150.

## 6. Conclusions

The results of this paper show that SPH simulations using a standard algorithm reproduce the results obtained by other researchers for decaying turbulence in a square box with no-slip boundary conditions provided the initial particle spacing is $>1/125$, in agreement with estimates made using the Reynolds number. These results include the time variation of the decay of kinetic energy, enstrophy and the form of the second and fourth order velocity correlation functions. In calculations not described here we show that the remarkable changes in the angular momentum discovered by Clercx et al. [20] (see also [26]) are also reproduced. The turbulence model proposed in this paper not only reproduces these results but, in addition, shows that quantities such as the second order velocity correlation function calculated with an initial particle spacing of 1/150, can be reproduced with an initial particle spacing 1/75 which requires a factor 8 less computation to integrate to a specified time. The new algorithm is easy to implement and requires typically only 20% more computing time than a standard integration. An attractive feature of the algorithm is that, like the LANS-$\alpha$ model, it conserves linear and angular momentum (in the absence of fixed bodies or boundaries and external forces), and satisfies a discrete form of Kelvin's circulation theorem.

Within the framework of two-dimensional flow their are interesting problems whose solution will clarify features of the turbulence model. These include driven turbulence which we intend to explore using mechanical stirring since SPH allows the combination of moving bodies and fluids to be treated easily. An example is a set of rods moving in the square box as in the experiment of Maassen et al. [24], but with rods that can move independently. Another class of problems already considered by Wells et al. [36] is the development of vorticity near boundaries [23] and the collision of dipole vortex distributions with walls.

The turbulence model can be extended easily to simulate turbulence in pipes and channels as in the applications of the alpha model by Chen et al. [8]. This will determine the ability of the model to reproduce turbulence near walls and in the bulk of the fluid. Other applications include the effect of turbulence in sloshing tanks where turbulence is generated by breaking waves, and the swimming of linked bodies [37].

The SPH simulation of gas dynamics, especially in astrophysics, requires simulating turbulence when the density and the resolution vary in space and time. Because the density changes the lengths $\ell$ or $h$ change since it is normal for $h \propto 1/\rho^{1/d}$ where $d$ is the number of dimensions. The analysis in this paper can be extended to take account of this variation with the result that an extra stress term appears in the acceleration equation. Planned work includes simulations of turbulent disk like structures and star formation that are of importance in astrophysics.

## Acknowledgment

This research was funded with the support of ARC Discovery grant DP0881447 (Analysis of two-phase sloshing in marine tanks).

## Appendix. Lagrange's equations

Lagrange's equations for particle $c$ are

$$\frac{\mathrm{d}}{\mathrm{d}t}\left(\frac{\partial L}{\partial \widehat{\mathbf{v}}_c}\right) = \frac{\partial L}{\partial \mathbf{r}_c}. \tag{A.1}$$

The Lagrangian must therefore be written in terms of the $\widehat{\mathbf{v}}$ and $\mathbf{r}$. In order to do this it is convenient to write the smoothing equation (2.17) in the form

$$\widehat{\mathbf{p}}_a = m_a\widehat{\mathbf{v}}_a = \sum_b D_{ab}\mathbf{v}_b, \tag{A.2}$$

where the subscripts denote particle labels, and

$$D_{ab} = \delta_{ab}\left(m_a - \epsilon\sum_{j\neq a}\sigma_{aj}K_{aj}\right) + \epsilon(1-\delta_{ab})\sigma_{ab}K_{ab}, \tag{A.3}$$

$\sigma_{ab} = m_a m_b/M$, and $\delta_{ab}$ is the Kronecker delta. Note that $D_{ab}$ is symmetric and the matrix $\mathbf{D}$ with elements $D_{ab}$ is a square, symmetric matrix. We can then write

$$\mathbf{v}_a = \sum_b (D)^{-1}_{ab}\widehat{\mathbf{p}}_b, \tag{A.4}$$

where $(D)^{-1}_{ab}$ is the $ab$ component of the matrix inverse to $D$. The kinetic energy component of $L$

$$E_K = \frac{1}{2}\sum_a m_a\widehat{\mathbf{v}}_a\cdot\mathbf{v}_a, \tag{A.5}$$

can then be written in the form

$$E_K = \frac{1}{2}\sum_a \widehat{\mathbf{p}}_a\cdot\sum_b (D)^{-1}_{ab}\widehat{\mathbf{p}}_b. \tag{A.6}$$

The canonical momentum is given by

$$\frac{\partial E_K}{\partial \widehat{\mathbf{v}}_c} = \frac{1}{2}\sum_a\sum_b (m_a\delta_{ac}\widehat{\mathbf{p}}_b + m_b\delta_{bc}\widehat{\mathbf{p}}_a)D^{-1}_{ab} = m_c\mathbf{v}_c, \tag{A.7}$$

because the first and second terms in the summation are identical, and both equal to $\frac{1}{2}m_c\mathbf{v}_c$.

The right hand side of Lagrange's equations (A.1) has two contributions, one from kinetic energy term and one from the internal energy. The second leads to the usual SPH pressure equations (see for example [38,1]). The first can be written

$$\frac{\partial E_K}{\partial \mathbf{r}_c} = \frac{1}{2}\frac{\partial}{\partial \mathbf{r}_c}\left(\widehat{\mathbf{p}}\,\mathbf{D}^{-1}\widehat{\mathbf{p}}\right) = \frac{1}{2}\widehat{\mathbf{p}}\left(\frac{\partial}{\partial \mathbf{r}_c}\mathbf{D}^{-1}\right)\widehat{\mathbf{p}}, \tag{A.8}$$

where $\widehat{\mathbf{p}} = (\widehat{\mathbf{p}}_1, \widehat{\mathbf{p}}_2, \widehat{\mathbf{p}}_3, \ldots)$, and the subscript denotes a particle label. The row or column form is taken as required for the matrix products. The derivative $\partial/\partial\mathbf{r}_c$ is to be interpreted in terms of a separate matrix equation for each component of $\mathbf{r}_c$. Because $\mathbf{D}$ is a square symmetric matrix so is its inverse, and we can use the identity

$$\frac{\partial}{\partial \mathbf{r}_c}\mathbf{D}^{-1} = -\mathbf{D}^{-1}\left(\frac{\partial}{\partial \mathbf{r}_c}\mathbf{D}\right)\mathbf{D}^{-1}. \tag{A.9}$$

If this result is substituted into (A.8) and note is taken of (A.4), we can write (A.8) as

$$\frac{\partial E_K}{\partial \mathbf{r}_c} = -\frac{1}{2}\mathbf{v}\left(\frac{\partial \mathbf{D}}{\partial \mathbf{r}_c}\right)\mathbf{v}, \tag{A.10}$$

where $\mathbf{v} = (\mathbf{v}_1, \mathbf{v}_2, \mathbf{v}_3, \ldots)$ and in (A.10) the row or column vector form is used as needed. We can then write

$$\frac{\partial E_K}{\partial \mathbf{r}_c} = -\frac{1}{2}\sum_a \sum_b \mathbf{v}_a \cdot \mathbf{v}_b \left(\frac{\partial D_{ab}}{\partial \mathbf{r}_c}\right). \tag{A.11}$$

The expression (A.3) for $D_{ab}$ contains two summation terms. The first is

$$D^{(1)}_{ab} = \delta_{ab}\left(m_a - \epsilon \sum_{j\neq a} \sigma_{aj} K_{aj}\right), \tag{A.12}$$

with derivative

$$\frac{\partial D^{(1)}_{ab}}{\partial \mathbf{r}_c} = -\epsilon \delta_{ab} \sum_{j\neq a} \sigma_{aj} \frac{\partial K_{aj}}{\partial \mathbf{r}_a}(\delta_{ac} - \delta_{jc}). \tag{A.13}$$

Note that, as mentioned earlier, $\ell_{ab}$ can be considered constant when calculating the spatial derivative of $K_{aj}$. The contribution to the derivative of the kinetic energy is

$$\frac{\partial E^{(1)}_K}{\partial \mathbf{r}_c} = \frac{1}{2}\epsilon \sum_a \sum_b \mathbf{v}_a \cdot \mathbf{v}_b \delta_{ab} \sum_{j\neq a} \sigma_{aj} \frac{\partial K_{aj}}{\partial \mathbf{r}_a}(\delta_{ac} - \delta_{jc}). \tag{A.14}$$

If this expression is simplified, noting that $\partial K_{ab}/\partial \mathbf{r}_a = -\partial K_{ab}/\partial \mathbf{r}_b$, it becomes

$$\frac{\partial E^{(1)}_K}{\partial \mathbf{r}_c} = \frac{1}{2}\epsilon \sum_{a\neq c} (v_a^2 + v_c^2)\sigma_{ac} \frac{\partial K_{ac}}{\partial \mathbf{r}_c}. \tag{A.15}$$

The second contribution to $D_{ab}$ is

$$D^{(2)}_{ab} = \epsilon(1 - \delta_{ab})\sigma_{ab} K_{ab} \tag{A.16}$$

with derivative

$$\frac{\partial D^{(2)}_{ab}}{\partial \mathbf{r}_c} = \epsilon(1 - \delta_{ab})\sigma_{ab} \frac{\partial K_{ab}}{\partial \mathbf{r}_a}(\delta_{ac} - \delta_{bc}), \tag{A.17}$$

and the contribution to the derivative of the kinetic energy is

$$\frac{\partial E^{(2)}_K}{\partial \mathbf{r}_c} = -\frac{1}{2}\epsilon \sum_a \sum_b \mathbf{v}_a \cdot \mathbf{v_b}(1 - \delta_{ab})\sigma_{ab} \frac{\partial K_{ab}}{\partial \mathbf{r}_a}(\delta_{ac} - \delta_{bc}). \tag{A.18}$$

If this expression is simplified it can be written

$$\frac{\partial E^{(2)}_K}{\partial \mathbf{r}_c} = -\epsilon \sum_{a\neq c} \sigma_{ac} \mathbf{v}_a \cdot \mathbf{v}_c \frac{\partial K_{ac}}{\partial \mathbf{r}_c}. \tag{A.19}$$

Combining (A.15) and (A.19) gives

$$\frac{\partial E_K}{\partial \mathbf{r}_c} = \frac{1}{2}\epsilon \sum_{a\neq c} v_{ac}^2 \sigma_{ac} \frac{\partial K_{ac}}{\partial \mathbf{r}_c}, \tag{A.20}$$

where $\mathbf{v}_{ac} = \mathbf{v}_a - \mathbf{v}_c$. The result (A.20) shows that the force terms arising from the smoothing are Galilean invariant.

The contribution to the equations of motion from the internal energy term can be calculated easily [38,1] using either a summation form for the density (appropriate to astrophysical applications) or using the continuity equation as a constraint. In the present case we assume the fluid is homogeneous, and we use the continuity equation for a particle $c$ in the form

$$\frac{\mathrm{d}\rho_c}{\mathrm{d}t} = \sum_b m_b \widehat{\mathbf{v}}_{cb} \cdot \nabla_c W_{cb}, \tag{A.21}$$

where $W$ is a kernel similar in form to $G$. Lagrange's equation for particle $c$ become

$$\frac{\mathrm{d}\mathbf{v}_c}{\mathrm{d}t} = -\sum_b m_b \left(\frac{P_c}{\rho_c^2} + \frac{P_b}{\rho_b^2}\right)\nabla_c W_{cb} + \frac{\epsilon}{2}\sum_b \frac{m_b}{M} v_{cb}^2 \nabla_c K_{cb}. \tag{A.22}$$

## References


[1] J.J. Monaghan, Smoothed particle hydrodynamics, Rep. Prog. Phys. (2005).
[2] J.J. Monaghan, Simulating free surface flows with SPH, J. Comput. Phys. 110 (1994) 399–406.
[3] S.J. Cummins, M. Rudman, Using an approximate projection method to model incompressible flows in SPH, J. Computat. Phys. 152 (1999) 584–607.
[4] X.Y. Hu, N.A. Adams, An incompressible multi-phase SPH method, J. Comput. Phys. 227 (2007) 264–278.
[5] D. Violeau, R. Issa, Numerical modelling of complex turbulent free surface flows with the SPH method: an overview, Int. J. Numer. Methods 53 (2007) 277–304.
[6] D.D. Holm, Fluctuation effects on 3D Lagrangian mean and Eulerian mean fluid motion, Physica 133 (1999) 215–269.
[7] D.D. Holm, Physica D 170 (2002) 253.
[8] S. Chen, C. Foias, D.D. Holm, E. Olson, E.S. Titi, S. Wynne, A connection between the Camassa–Holm equations and turbulent flows in channels and pipes, Phys. Fluids 11 (8) (1999) 2343–2353.
[9] S. Chen, D.D. Holm, L.G. Margolin, R. Zhang, Direct numerical simulations of the Navier Stokes alpha model, Physica D 133 (1999) 66–83.
[10] A. Cheskidov, Darryl D. Holm, Eric Olson, Edriss S. Titi, On a Leray-$\alpha$ model of turbulence, Proc. Phys. Soc. 461 (2005) 629–649.
[11] Bernard J. Geurts, Darryl D. Holm, Leray and LANS-$\alpha$ modelling of turbulent mixing, J. Turbul. 7 (10) (2006) 1–33.
[12] K. Moheseni, B. Kozovic, S. Shkoller, J.E. Marsden, Numerical simulations of the Lagrangian averaged Navier–Stokes equations for homogeneous isotropic turbulence, Phys. Fluids 15 (2003) 524.
[13] Jonathan Pietarila Graham, Darryl D. Holm, Pablo D. Miinni, Annick Pouquet, Highly turbulent solutions of the Lagrangian-averaged Navier–Stokes $\alpha$ model and their large-eddy-simulation potential, Phys. Rev. E. 76 (2007) 056310.
[14] E. Lunasin, S. Kurien, M.A. Taylor, E.S. Titi, A study of the Navier Stokes model for two dimensional turbulence, J. Turbul. 8 (30) (2007) 1–21.
[15] Evelyn Lunasin, Susan Kurien, Edriss S. Titi, Spectral scaling of the Leray-$\alpha$ model for two dimensional turbulence, J. Phys. A. Math. Theor. 41 (2008) 344014.
[16] J.J. Monaghan, SPH simulations of shear flow, Mon. Not. R. Astron. Soc. 365 (1) (2006) 199–213.
[17] J.J. Monaghan, J.B. Kajtar, SPH particle boundary forces for arbitrary boundaries, Computer Physics Comm. 180 (2009) 1811–1820.
[18] C.S. Peskin, Numerical analysis of blood flow in the heart, J. Comput. Phys. 25 (1977) 220–252.
[19] C.S. Peskin, The immersed boundary method, Acta Numer. 10 (2002) 479–517.
[20] H.J.H. Clercx, S.R. Maassen, G.J.F. van Heijst, Spontaneous spin-up during the decay of 2D turbulence in a square container with rigid boundaries, Phys. Rev. Ltr. 80 (1998) 5129–5132.
[21] H.J.H. Clercx, S.R. Maassen, G.J.F. van Heijst, Decaying two-dimensional turbulence in square containers with no-slip or stree-free boundaries, Phys. Fluids 11 (3) (1999) 611–626.
[22] H.J.H. Clercx, G.J.F. Heijst, Energy spectra for decaying two dimensional turbulence in a bounded domain, Phys. Rev. Lett. 85 (2) (2000) 306–309.
[23] H.J.H. Clercx, C.-H. Bruneau, The normal and oblique collison of a dipole with a no-slip boundary, Comput. Fluids 35 (2006) 245–279.
[24] S.R. Maassen, H.J.H. Clercx, G.J.F. Heijst, Self organization of quasi-two dimensinal turbulence in stratified fluids in square and circular containers, Phys. Fluids 14 (7) (2002) 2150–2169.
[25] H.J.H. Clercx, A.H. Nielsen, D.J. Torres, E.A. Cortsias, Two dimensional turbulence in square and circular domains with no-slip walls, Eur. J. Mech. B/Fluids 20 (2001) 557–576.
[26] G.J.F. Van Heijst, H.J.H. Clercx, D. Molenaar, The effects of solid boundaries on confined two-dimensional turbulence, J. Fluid Mech. 554 (2006) 411–431.
[27] C. Eckart, Variation principles of hydrodynamics, Phys. Fluids 3 (1960) 421.
[28] C. Foias, D.D. Holm, E.S. Titi, The Navier–Stokes alpha model of turbulence, Physica D 152 (2001) 505–519.
[29] J.J. Monaghan, SPH Compressible turbulence, Mon. Not. R. Astron. Soc. 335 (2002) 843–852.
[30] Matthew Hecht, Darryl D. Holm, Mark R. Peterson, Beth A. Wingate, Implementation of the LANS-$\alpha$ turbulence model in a primitive ocean model, J. Comput. Phys. 227 (11) (2008) 5691–5716.
[31] J.J. Monaghan, On the problem of penetration in particle methods, J. Comput. Phys. 82 (1989) 1–15.
[32] H. Wendland, Piecewise polynomial, positive definite, and compactly supported radial functions of minimal degree, Adv. Comput. Math. 4 (1995) 389–396.
[33] J.E. Marsden, M. West, Discrete mechanics and variational integrators, Acta Numer. 10 (1) (2001) 357–514.
[34] A. Babiano, C. Basdevant, R. Sadourny, Structure functions and dispersion laws in two-dimensional turbulence, J. Atmospheric Sci. 42 (1985) 941–949.
[35] R.H. Kraichnan, Inertial-ranges in two-dimensional turbulence, Phys. Fluids 10 (1967) 1417–1423.
[36] M.G. Wells, H.J.H. Clercx, G.J.F. Heijst, Vortices in oscillating spin up, J. Fluid Mech. 573 (2007) 339–369.
[37] J. Kajtar, J.J. Monaghan, SPH simulations of swimming linked bodies, J. Comput. Phys. 227 (2008) 8568–8587.
[38] J.J. Monaghan, Smoothed particle hydrodynamics, Ann. Rev. Astron. Astrophys. 30 (1992) 543.